# The Role of Moisture Conveyor Belts for Precipitation in the Atacama Desert

**Christoph Böhm**[1] 📧, **Mark Reyers**[1] 📧, **Leon Knarr**[1] 📧, **and Susanne Crewell**[1] 📧

[1]Institute for Geophysics and Meteorology, University of Cologne, Cologne, Germany

**Abstract** In the hyperarid Atacama Desert in northern Chile, rare precipitation events can leave long-lasting geomorphological traces and have strong impacts on biota. While moisture conveyor belts (MCBs) and atmospheric rivers (ARs) have been associated with extreme precipitation in semiarid regions, their role for the Atacama Desert has not been previously investigated. This study reveals that about four MCBs per year make landfall in the Atacama Desert. According to simulated precipitation, 40–80% of the total precipitation between the coast and the Andean foothills is associated with MCBs. A case study reveals an elevated moisture transport decoupled from the maritime boundary layer, which is generalized by a composite analysis. Back trajectories reveal the Amazon Basin as the main source of moisture. MCB landfall times are derived from the AR catalog by Guan and Waliser (2015), https://doi.org/10.1002/2015jd024257. Implications of the results on paleoclimate reconstructions are discussed.

**Plain Language Summary** In the extremely dry Atacama Desert in northern Chile, rare rain events can trigger landscape alterations and have strong impacts on various life forms. Traces of such events are conserved within the desert soil over long time periods throughout the enduring dryness. Such traces constitute climate archives, which can be excavated and explored. Understanding particular conditions, which lead to extreme precipitation events is necessary to interpret such archives, reconstruct climate history, and explore thresholds of life at the dry limit. In this study, the role of a weather phenomenon called moisture conveyor belt (MCB) is quantified for the first time for the Atacama Desert. It is demonstrated that depending on region, 40–80% of the total rainfall is associated with these phenomena. In contrast to atmospheric river characteristics reported for midlatitudes, a unique vertical structure with an elevated moisture transport independent of the near-surface layer is discovered here. Even though the identified MCBs approach the Atacama Desert from northwesterly directions across the Pacific Ocean, the associated moisture mostly originates from the Amazon Basin.

## 1. Introduction

In the Atacama Desert, which is characterized by extreme hyperaridity, rarely occurring precipitation events are the dominant driver for fluvial alterations of the landscape through landslides and debris flow (e.g., Haug et al., 2010; Jordan et al., 2019; Vargas et al., 2006; Walk et al., 2020). Precipitation can also activate soil microbial communities (Jones et al., 2018), trigger germination of various species (Pliscoff et al., 2017), and cause the spectacular "blooming desert" (Astorga-Eló et al., 2020; Chávez et al., 2019). Traces of such biological and geological processes are manifested and preserved in climate archives (Bartz et al., 2020; Diederich et al., 2020; Ritter et al., 2019). To interpret such archives and reconstruct climate history, it is necessary to identify synoptic drivers for precipitation and understand the underlying mechanisms. With a very limited observational basis for this region, a solid comprehension has been hampered to date. While synoptic drivers, such as cutoff lows and troughs, have been discussed in previous studies (e.g., Jacques-Coper et al., 2015; Montecinos & Aceituno, 2003; Reyers et al., 2020), the role of moisture conveyor belts (MCBs; Knippertz & Martin, 2007) for the Atacama Desert has not been investigated so far.

Knippertz and Martin (2007) defined MCBs as elongated bands of enhanced poleward water vapor fluxes above the planetary boundary layer that are rooted in the Tropics. They can form when a trough or a cutoff low located above the maritime boundary layer (MBL) at very low latitudes is tapping the vertically extended tropical moisture pool by inducing a poleward flow. Upon landfall, MCBs are directly associated or in connection with atmospheric rivers (ARs; American Meteorological Society, 2021) to precipitation extremes, flooding, and landslides (Bao et al., 2006; Knippertz & Martin, 2007; Stohl et al., 2008).

Due to the similar filamentary structure of MCBs and ARs visible, for example, in fields of integrated water vapor transport (IVT), state-of-the-art AR detection algorithms may not distinguish these features. Intriguingly, a few declared "AR" landfalls have been detected for northern Chile (Guan & Waliser, 2015, their Figure 8). Despite the similar structure, there are conceptual differences. ARs are typically linked to a low-level jet and an extratropical cyclonic frontal system (Ralph et al., 2018), whereas MCBs are dominated by latent rather than sensible heat transport often without strong frontal zones acting in tropical or subtropical regimes (Knippertz & Martin, 2007). Therefore, MCB appears to be the more appropriate term for the objects identified for the Atacama region. Additionally, the described concept of MCBs is consistent with previous studies, which linked extreme precipitation to mid-tropospheric moisture transport (Reyers et al., 2020).

With the transport being presumably limited to the free troposphere, the moisture reaching the Atacama Desert is likely of remote origins. Recent studies indicate the tropical Pacific and the Amazon Basin as potential sources (Jordan et al., 2019; Reyers et al., 2020). In this study, the role of MCBs for precipitation in the Atacama Desert and the underlying mechanisms is studied under three overarching hypothesis:

1. A substantial amount of precipitation within the Atacama Desert is due to MCBs.
2. The main origin of the MCB-related moisture is the Amazon Basin.
3. MCB-related moisture transport and precipitation formation mostly take place in mid- and upper-tropospheric layers and are decoupled from the MBL.

## 2. Data

### 2.1. MCB Identification

To identify the times of MCB landfalls at the coast of the Atacama Desert, we use the AR catalog by Guan and Waliser (2015). The AR identification algorithm considers a percentile-based IVT threshold to identify objects of interest, which are further tested against orientation and geometry criteria. This ensures that even in very dry subtropical regimes, MCBs can be identified as ARs due to their similar shape within IVT fields. Discriminating characteristics such as the tropical moisture tapping for MCBs or the relation to a low-level jet along a cold front for ARs are not considered by the algorithm allowing MCBs to be included in the identification. The catalog is maintained with frequent updates and improvements of the identification algorithm (https://ucla.box.com/ARcatalog; Guan et al., 2018). Here, Version 2, available for different reanalysis data sets, is applied (Guan, 2020). By choosing the AR data set based on ERA-Interim (Dee et al., 2011), consistency with an ERA-Interim-driven Weather Research and Forecasting Model (WRF) simulation (Section 2.2) is ensured. The data set is provided at a 6-hr temporal resolution on a 1.5° by 1.5° grid.

Identified objects are filtered for those which made landfall at the coast of the Atacama Desert between 17°S and 30°S. If two consecutive landfalls are at least 48 hr apart, they are counted as separate MCBs. A total of 172 landfalls are detected for the period between 1979 and 2019, which average to about 4.2 per year. Most MCBs make landfall around 24°S (1.3 per year) and 30°S (1.1 per year, Figure S1 in Supporting Information S1). Monthly counts reveal a distinct seasonal cycle with the most active season between May and September and only a total of 12 landfalls between November and February within the 41-year period (Figure S2 in Supporting Information S1).

### 2.2. Regional Climate Model and Precipitation Observations

Precipitation and auxiliary data (relative humidity, wind, and cloud liquid water) are taken from a simulation with the regional climate model WRF (Reyers, 2018). The data set comprises daily accumulated precipitation at a 10 -km resolution for a 36-year period (1982–2017). For the simulation, a double one-way nesting is applied using ERA-Interim as boundary conditions. The inner domain roughly spans the region between 16°S–26°S and 74°W–67°W (see Reyers et al., 2020).

The climatology of the simulated precipitation reveals a hyperarid core region roughly between 18°S and 24°S below 2,000 -m altitude with annual rainfall below 4 mm (Figure S3 in Supporting Information S1). Following a steep topographic gradient (Shuttle Radar Topographic Mission data; Farr et al., 2007), mean annual precipitation rates rapidly increase toward the Altiplano in the northeast, which is consistent with the results from previous studies (e.g., Houston & Hartley, 2003; Houston, 2006). A validation of the
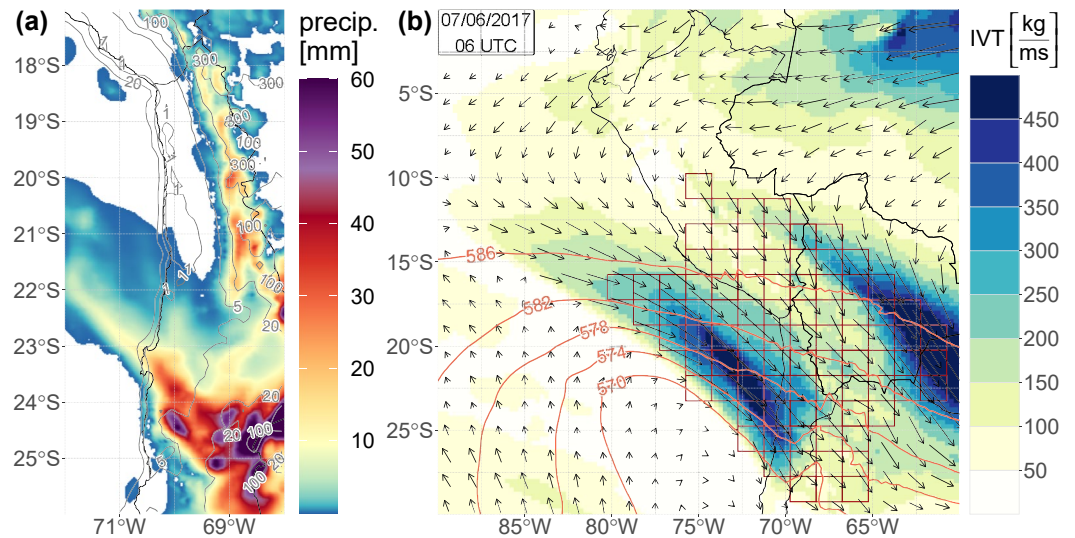
**Figure 1.** (a) Weather Research and Forecasting Model and CR2 station (magenta circles) 2-day precipitation sum for 6–7 June 2017 (color scale) and mean annual precipitation in mm (contour lines). (b) Integrated water vapor transport (IVT) between 850 hPa and 200 hPa (color shading and arrows), geopotential height in 500 hPa (light red contours), and MCB shape according to the applied AR catalog (dark red boxes) for June 7, 2017 at 6 UTC.

precipitation data set against gauge measurements provided by CR2 (Center for Climate and Resilience Research, 2018) shows suitable accuracy of the model (Reyers et al., 2020). In addition to the CR2 data set, more recent gauge observations are obtained (http://explorador.cr2.cl; Center for Climate and Resilience Research, 2019) to further assess the validity of the modeled precipitation (Section 3).

### 2.3. Reanalysis and Radiosounding Data

Data from the European Centre for Medium-Ranged Weather Forecast's (ECMWF) 5th generation reanalysis (ERA5; Hersbach et al., 2020) are utilized for a composite analysis. Surface pressure, mean sea-level pressure, integrated water vapor (IWV), and variables on pressure levels (geopotential height, temperature, specific humidity, and horizontal wind) are obtained as hourly fields with a spatial resolution of 0.25° of longitude and latitude. The total water vapor transport $\overline{Q}$ between two pressure levels $p_{\text{bot}}$ and $p_{\text{top}}$ (usually 850 hPa and 200 hPa, respectively) is calculated using the horizontal wind vector $\overline{U} = (u, v)$, the specific humidity $q$, and the gravitational acceleration $g$ of the Earth:

$$\overline{Q} = \frac{1}{g} \int_{p_{\text{bot}}}^{p_{top}} q\overline{U} \cdot \mathrm{d}p \tag{1}$$

ERA5 data are further applied to derive 7-day backward trajectories of air parcels arriving at the Atacama Desert around MCB-landfall times. Herein, the Hybrid Single Particle Lagrangian Integrated Trajectory Model (HYSPLIT, https://www.arl.noaa.gov/hysplit/, National Oceanic and Atmospheric Administration Air Resources Laboratory; Stein et al., 2016) is run using hourly 3D fields of meteorological data. Furthermore, radiosonde data available for daily launches at 12 UTC are obtained from the Integrated Global Radiosonde Archive (IGRA; Durre et al., 2016) for Antofagasta (23.5°S, 70.4°W).

## 3. Case Study

A heavy precipitation event occurred in June 2017 within the hyperarid core of the Atacama Desert. Accumulated precipitation for 6–7 June 2017 exceeded 30 mm in a band of roughly 50 -km width, which stretched from the Mejillones Peninsula southeastward toward the Andean Precordillera in both the model and the gauge observations (Figure 1a). Some regions received rain amounts even higher than 50 mm,

which surpasses the tenfold mean annual precipitation rate. In the course of the event, various microbial species vanished due to the ponding of a lagoon near Yungay (Azua-Bustos et al., 2018).

The event was associated with a mid-tropospheric trough, which anomalously occurred far north and approached the Atacama Desert from the west (Figure 1b). Ahead of the trough, a strong water vapor transport along the Peruvian coast toward the Atacama Desert could be identified as an MCB.

The disturbance only affected tropospheric levels above the MBL, whereas the prevailing southeast Pacific anticyclone remained intact at the surface (Figure S4 in Supporting Information S1). In fact, the IVT integrated between the surface and 850 hPa has a northward component. This indicates that the relevant moisture transport is limited to the free troposphere. Trajectories for this event show a southerly inflow for lower target heights (500 and 1,000 m), reflecting the near-surface anticyclone (Figure S5 in Supporting Information S1). For higher target heights, a northwesterly inflow along the Peruvian coast originally stemming from the Amazon Basin is revealed.

Longitude-height cross sections across the main precipitation band show that the MBL and a humid layer at the verge of saturation above 5 km are separated by a layer of very low relative humidity (Figures S6a and S6c in Supporting Information S1). This indicates that there is no significant exchange between the upper moist layer and the MBL. Furthermore, the strongest winds are collocated with the elevated moisture peak. Thus, the main moisture transport toward the Atacama Desert appears to be decoupled from the MBL and is realized at mid-tropospheric heights, so that it can cross the coastal mountain range.

With heights between 1,500 m and 2,500 m, the coastal mountain range introduces a vertical wind component, which is transferred to higher altitudes. The resulting lifting of the moist air leads to cloud formation manifested in enhanced cloud liquid water (Figures S6a and S6c in Supporting Information S1). At a later stage of the event, the dynamics of the accompanying trough result in a more complex circulation, which allows downward mixing of moisture and cooling of the lower layer. This is indicated by higher relative humidity at lower altitudes over land and further cloud formation (Figures S6b and S6d in Supporting Information S1).

Radiosondes launched within 2–6 June 2017 reveal that the temperature inversion monotonically weakened (Figure S7a Supporting Information S1), which can be attributed to the approach of the mid-tropospheric trough. Specific humidity slightly increased in the MBL and considerably between 450 and 750 hPa, whereas a layer right above the temperature inversion at around 850 hPa remained dry (Figure S7b in Supporting Information S1). This is consistent with the dry layer revealed by the WRF simulation and confirms that the MBL is decoupled from the moisture accumulation within higher layers. The latter is explained by the increasing inland water vapor flux, leading to the precipitation event (Figures S7c and S7d in Supporting Information S1).

A recently established weather station (Cerros de Calate; 21.4°S, 69, 8°W) reveals the onset of the rainfall period at 1 UTC and the end at 6:30 UTC on June 7, 2017 with 0.7 mm in total (Hoffmeister, 2017). Therefore, the radiosounding profile for June 7, 2017 at 12 UTC (8 a.m. local time) unveils the situation a few hours after the precipitation event. Only then, the temperature inversion has dissipated. This is likely due to evaporative cooling upon descending water droplets, which is consistent with the observed moistening of the dry layer around 850 hPa (Figure S7 in Supporting Information S1). An onshore vertical homogenization of the relative humidity is also indicated by the simulation (Figures S6b and S6d in Supporting Information S1).

## 4. Composite Analysis

For the 36-year period (1982–2017) covered by the WRF simulation, 521 days that are related to landfalling MCBs are determined, including the day before and after. MCB-related precipitation is derived from the WRF precipitation data set. Composite mean fields (sea-level pressure and geopotential height), mean vertical profiles (temperature, specific humidity, and water vapor flux), and anomalies (IWV) are derived from ERA5 data.
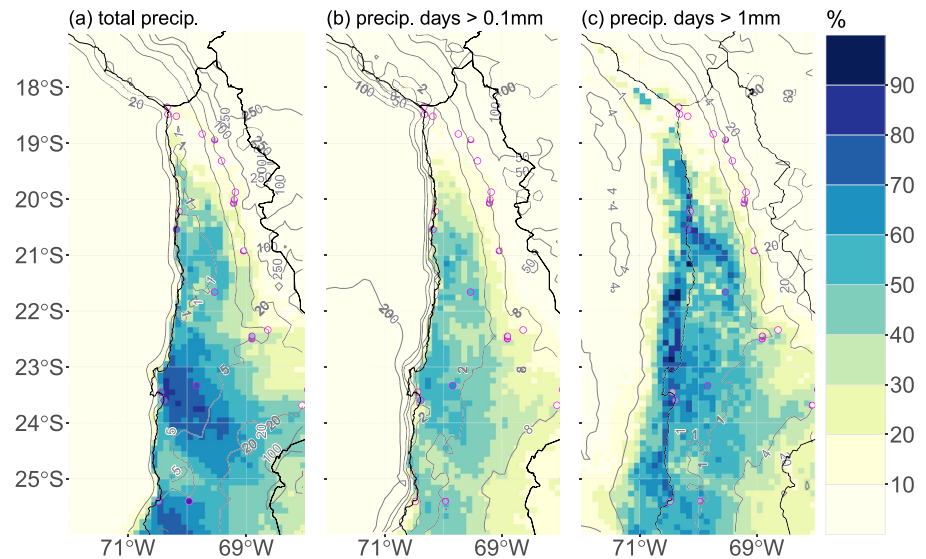
**Figure 2.** Moisture conveyor belts (MCB)-related fraction of (a) total precipitation amount, (b) days with precipitation greater than 0.1 mm, and (c) days with precipitation greater than 1 mm based on a WRF simulation (Reyers et al., 2020). Contour lines represent the annual mean for each variable. Circles denote the respective analysis based on gauge measurement (source: CR2).

The MCB-related fraction of total precipitation exceeds 40% for most of the Atacama Desert south of 20°S (Figure 2a). An overall gradient between higher fractions in the southwest and lower fractions in the northeast is consistent with the decrease of MCB-landfall frequency from south to north (Figure S1 in Supporting Information S1) and the increase of summertime convection toward the Altiplano in the northeast (Garreaud, 1999). Maximum fractional precipitation appears in an area between 23°S and 24°S bounded by the city of Antofagasta in the west, stretching into the central valley to the east and just slightly north of the European Southern Observatory's construction site for the world's largest optical telescope (Cantalloube et al., 2020; Ramsay et al., 2020). For this region, more than 70% of the total precipitation is associated with MCBs making landfall. These findings demonstrate the importance of MCBs for precipitation in the Atacama.

Precipitation events are rare in the Atacama Desert, which means that some locations do not receive any rain within several years (Cereceda et al., 2008). Therefore, the fraction of days with precipitation is another quantity, which characterizes the impact of MCBs for this region. More than a third out of all days with detectable precipitation (greater than 0.1 mm) is associated with an MCB landfall for most of the Atacama Desert south of 20°S (Figure 2b). If the threshold is increased to 1 mm, the MCB-related fraction increases with values exceeding 50% for most parts (Figure 2c). In other words, days with higher precipitation amounts are more likely to be MCB related. Since it requires stronger events to trigger mudslides or debris flow both causing landscape evolution detectable in paleoclimate archives (Vargas et al., 2006), such archives may strongly reflect MCB activity.

The composite analysis reveals that similar to the case study, MCBs are typically associated with an upper-level trough ahead of the coast (Figure S8 in Supporting Information S1). Additionally, IWV is enhanced across the southeast Pacific with the highest positive anomaly a few hundred kilometers west of the coast of northern Chile. A northwesterly airflow at the foreside of this trough potentially transports this moisture excess toward the Atacama Desert. The southeast Pacific anticyclone is still visible according to mean sea-level pressure, which means that the prevailing southerlies within the MBL along the Chilean coast remain present in most MCB cases.

To investigate the vertical structure of the atmosphere under MCB conditions, the vertical column with maximum absolute IVT is identified for each MCB-related day. The composite mean and the standard deviation of vertical profiles are compared to seasonal climatologies (Figures 3a and 3b). Under MCB conditions, the
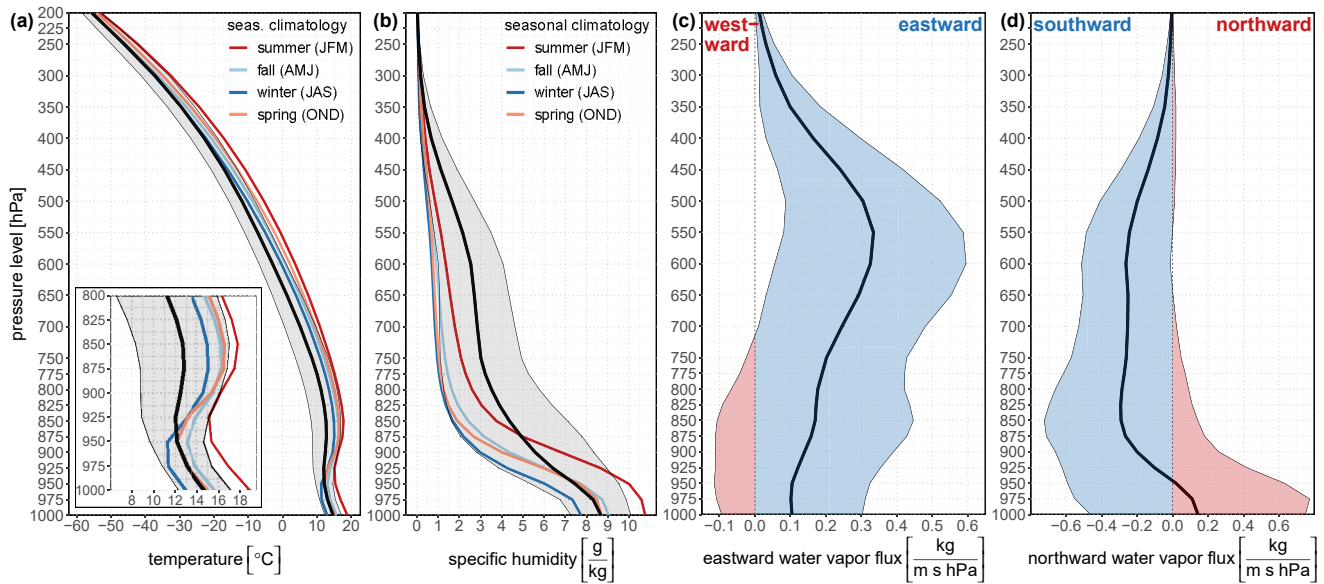
**Figure 3.** Moisture conveyor belts (MCB)-composite vertical profiles of (a) temperature, (b) specific humidity, (c) eastward water vapor flux, and (d) northward water vapor flux. For each MCB, the ERA5 pixel with maximum IVT within a bounding box between 18°S–30°S and 73°W–71.5°W is selected for the calculation. MCB-composite mean (black line) and standard deviation (shaded) are denoted for each pressure level. Colored lines in (a) and (b) denote respective seasonal climatologies for the entire bounding box. Inlet in (a) zooms in on the temperature inversion.

temperature is considerably lower within the free troposphere compared to the mean of the coldest season (JAS, Figure 3a). Situations for the warm season are underrepresented in the MCB composite due to the seasonal distribution of MCB landfalls (Figure S2 in Supporting Information S1). Within the MBL, the composite mean temperature profile closely follows the seasonal average for spring and fall. This means, the inversion above the MBL is overall weakening during MCB events, which can be attributed to a reduced subsidence related to the presence of a mid-tropospheric trough.

For the composite mean-specific humidity profile, a strong enhancement in the mid- and upper troposphere compared to the seasonal climatologies is visible above 900 hPa (Figure 3b). Even though winter time (driest) situations are overrepresented, the MCB-related humidity profile exceeds the mean of the summer (wettest) season above 875 hPa. Overall, the enhancement of specific humidity is limited to the free troposphere.

The highest composite mean water vapor flux, connected with a southeastward transport, is observed between 4 and 5 km (600 and 550 hPa) on average (Figures 3c and 3d). While the zonal component remains positive across all pressure levels, the meridional component changes its direction for the lowest pressure levels. This can be expected, as the southeast Pacific anticyclone remains intact near the surface, supporting the prevailing southerlies along the Chilean coast (Figure S8 in Supporting Information S1).

To assess the origin of the air masses, 7-day back trajectories are calculated using the MCB landfall times as target times and the coastal pixels with maximum IVT as target locations. We only consider MCBs for an extended winter season between April and October to focus on the active MCB season (Figures S2 in Supporting Information S1). For lower target heights (1 km, 2 km, and 3 km), mainly northwesterly alongside zonal and southerly approaches toward the Atacama Desert are identified (Figure 4). The southerly direction is limited to the lowest trajectories. For higher target heights (4 km, 5 km, and 6 km), only northwesterly and westerly inflow directions appear (Figure 4b), consistent with the composite upper-level trough (Figure S8 in Supporting Information S1). For the northwesterly direction, the Amazon Basin constitutes the dominant origin.

For trajectories characterized by comparably low-specific humidity ("driest" tercile), the Pacific is the dominant origin (Figure 4c). Associated MCBs mostly make landfall in the southern Atacama. Trajectories characterized by comparably high specific humidity ("moistest" tercile) mainly originate from the Amazon
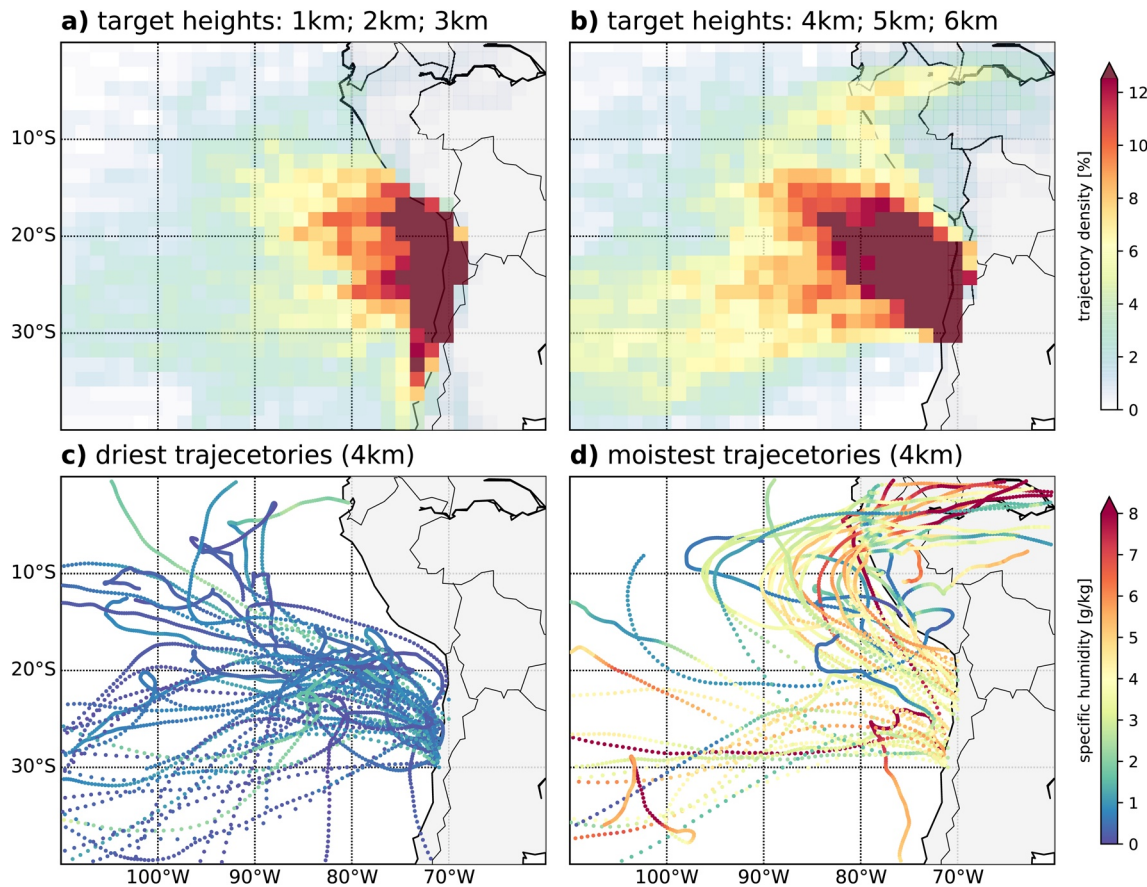
**Figure 4.** 7-day back trajectories for moisture conveyor belts-landfall times. Coastal pixels with maximum IVT between 850 hPa and 200 hPa are used as target locations. (a and b) Percentage of trajectories passing through the respective pixels for target heights above ground level of (a) 1 km, 2 km, 3 km and (b) 4 km, 5 km, 6 km. (c and d) Hourly values of specific humidity along selected trajectories with 4 -km target heights for which the mean-specific humidity of the last 6 hr before landfall time is (c) below the first tercile (driest third) and (d) above the second tercile (moistest third) of its distribution.

Basin (Figure 4d). These trajectories hardly indicate any moisture enrichment when they cross the Pacific Ocean. Therefore, the associated moisture is most likely from the Amazon Basin. Such moisture would essentially be of Atlantic origin (e.g., Garreaud et al., 2009). These very moist trajectories from the Amazon Basin are mostly associated with MCB landfalls in the hyperarid core (18°S–24°S).

## 5. Conclusion

In this study, the role of MCBs for the Atacama Desert is investigated. About 4 landfalls per year accumulate along the coast of northern Chile on average counting all landfalls between 17°S and 30°S. Even though the MCB landfall frequency is low, these synoptic features can have a substantial impact, considering the overall low precipitation rates for this hyperarid environment (<5 mm/year). For example, an MCB that made landfall on June 7, 2017 resulted in rainfall amounts, which exceeded average decadal rates (Figure 1a). Events of such scale presumably dominate the traces, which are identified in paleoclimate archives (Diederich et al., 2020; Jordan et al., 2019; Ritter et al., 2019).

For most regions of the Atacama Desert, more than 40% of the total precipitation is related to MCB landfalls. For a region east of Antofagasta, the fraction exceeds 70%. As the case study for the June 2017 MCB indicates, individual events can have a considerable impact on the spatial distribution. Given that a single MCB can be accounted for a decade's worth of rain, the 36-year long data record considered in this study appears quite short and should be extended.

Composite vertical profiles reveal that the moisture transport typically maximizes between 500 hPa and 600 hPa and is decoupled from the MBL. While a mid-tropospheric trough drives a northwesterly flow toward the Atacama Desert, the southeast Pacific anticyclone continues to drive southerlies along the coast near the surface. This is consistent with a previous description of MCBs for the North Pacific (Knippertz & Martin, 2007). The elevated structure identified here for the Atacama Desert demarcates these MCBs from ARs typically found in midlatitudes and high latitudes, for which the related water vapor flux typically peaks below 750 hPa (e.g., at 900 hPa for southern Chile; Guan & Waliser, 2015, their Figure 8b).

A trajectory analysis reveals that the most moisture-laden MCBs, which potentially lead to the strongest precipitation events, are sourced in the continental interior. The path leads from the Amazon Basin to the west, crosses the Andes most commonly between 3°S and 7°S, and turns southeastward over the tropical eastern Pacific to arrive at the Atacama Desert (Figure 4d). Similar pathways were identified for extreme precipitation events occurring during winter season in the southern, southeastern, and northern Atacama (Reyers et al., 2020). An isotopic analysis of rainwater and stream flows associated with the Atacama March 2015 flood (e.g. Bozkurt et al., 2016) indicated a tropical moisture source (Jordan et al., 2019). This is of interest because this event is also related to an MCB similar to the case study presented above. This further illustrates that the tropical and continental origin might be a common source region associated with MCB-related moisture.

The hyperarid core constitutes a biotic barrier (Ruhm et al., 2020) and climatic divide (Houston, 2006). Precipitation in the northeast is usually related to continental interior origin, whereas precipitation in the southwest is usually of Pacific origin (Houston, 2006; Houston & Hartley, 2003). Here, a third route is revealed, which is further supported by Jordan et al. (2019) and Reyers et al. (2020). To date, studies on paleoclimate reconstructions related to the Atacama Desert mostly consider sea surface temperature, latitudinal shifts of winter midlatitude westerlies, and cutoff lows in order to discuss implications from climate archives (Bartz et al., 2020; Diederich et al., 2020; Ritter et al., 2019). Wetter periods during the Pleistocene and Holocene are usually attributed to eastern or southwestern moisture sources (Jordan et al., 2019). An additional scenario, which should be considered to interpret implications of climate archives, is constituted by MCBs as discussed in this study.

## Data Availability Statement

ERA5 data (Hersbach et al., 2020) were downloaded from the Copernicus Climate Data Store (CDS) via Web-API. The utilized simulated precipitation data set is available at https://www.crc1211db.uni-koeln.de/search/view.php?dataID=38 (Reyers, 2018). Gauge measurements were retrieved from http://www.cr2.cl/datos-de-precipitacion/ (Center for Climate and Resilience Research, 2018) and from http://explorador.cr2.cl (Center for Climate and Resilience Research, 2019). The AR catalog version 2 data were produced based on ERA-Interim (Dee et al., 2011) according to the detection algorithm introduced by Guan and Waliser (2015) and Guan et al. (2018) and provided by Bin Guan via https://ucla.box.com/ARcatalog (Guan, 2020). Radiosonde data were obtained from the Integrated Global Radiosonde Archive (IGRA; Durre et al., 2016).

## References

American Meteorological Society. (2021). *Atmospheric river. Glossary of meteorology*. Retrieved from http://glossary.ametsoc.org/wiki/Atmospheric_river

Astorga-Eló, M., Zhang, Q., Larama, G., Stoll, A., Sadowsky, M. J., & Jorquera, M. A. (2020). Composition, predicted functions and co-occurrence networks of rhizobacterial communities impacting flowering desert events in the atacama desert, chile. *Frontiers in Microbiology*, *11*, 571–571. https://doi.org/10.3389/fmicb.2020.00571

Azua-Bustos, A., Fairén, A. G., González-Silva, C., Ascaso, C., Carrizo, D., Fernández-Martínez, M. Á., et al. (2018). Unprecedented rains decimate surface microbial communities in the hyperarid core of the Atacama desert. *Scientific Reports*, *8*(1), 16706. https://doi.org/10.1038/s41598-018-35051-w

Bao, J.-W., Michelson, S. A., Neiman, P. J., Ralph, F. M., & Wilczak, J. M. (2006). Interpretation of enhanced integrated water vapor bands associated with extratropical cyclones: Their formation and connection to tropical moisture. *Monthly Weather Review*, *134*(4), 1063–1080. https://doi.org/10.1175/MWR3123.1

Bartz, M., Walk, J., Binnie, S. A., Brill, D., Stauch, G., Lehmkuhl, F., et al. (2020). Late pleistocene alluvial fan evolution along the coastal Atacama desert (n Chile). *Global and Planetary Change*, *190*, 103091. https://doi.org/10.1016/j.gloplacha.2019.103091

Bozkurt, D., Rondanelli, R., Garreaud, R., & Arriagada, A. (2016). Impact of warmer eastern tropical pacific SST on the march 2015 Atacama floods. *Monthly Weather Review*, *144*(11), 4441–4460. https://doi.org/10.1175/MWR-D-16-0041.1

Cantalloube, F., Milli, J., Böhm, C., Crewell, S., Navarrete, J., Rehfeld, K., et al. (2020). The impact of climate change on astronomical observations. *Nature Astronomy*, *4*, 826–829. https://doi.org/10.1038/s41550-020-1203-3

Center for Climate and Resilience Research (2018). *Datos de precipitación*. Retrieved from http://www.cr2.cl/datos-de-precipitacion

Center for Climate and Resilience Research (2019). *Explorador climático*. Retrieved from http://explorador.cr2.cl

Cereceda, P., Larrain, H., Osses, P., Farías, M., & Egaña, I. (2008). The climate of the coast and fog zone in the Tarapacá region, Atacama Desert, Chile. *Atmospheric Research*, *87*(3), 301–311. https://doi.org/10.1016/j.atmosres.2007.11.011

Chávez, R., Moreira-Muñoz, A., Galleguillos, M., Olea, M., Aguayo, J., Latín, A., et al. (2019). Gimms ndvi time series reveal the extent, duration, and intensity of "blooming desert" events in the hyper-arid Atacama Desert, Northern Chile. *International Journal of Applied Earth Observation and Geoinformation*, *76*, 193–203. https://doi.org/10.1016/j.jag.2018.11.013

Dee, D. P., Uppala, S. M., Simmons, A. J., Berrisford, P., Poli, P., Kobayashi, S., et al. (2011). The era-interim reanalysis: Configuration and performance of the data assimilation system. *Quarterly Journal of the Royal Meteorological Society*, *137*(656), 553–597. https://doi.org/10.1002/qj.828

Diederich, J. L., Wennrich, V., Bao, R., Büttner, C., Bolten, A., Brill, D., et al. (2020). A 68 ka precipitation record from the hyperarid core of the Atacama Desert in Northern Chile. *Global and Planetary Change*, *184*, 103054. https://doi.org/10.1016/j.gloplacha.2019.103054

Durre, I., Xungang, Y., Vose, R. S., Applequist, S., & Arnfield, J. (2016). *Integrated global radiosonde archive (IGRA), version 2*. NOAA National Centers for Environmental Information. https://doi.org/10.7289/V5X63K0Q

Farr, T. G., Rosen, P. A., Caro, E., Crippen, R., Duren, R., Hensley, S., et al. (2007). The shuttle radar topography mission. *Reviews of Geophysics*, *45*(2). https://doi.org/10.1029/2005RG000183

Garreaud, R. (1999). Multiscale analysis of the summertime precipitation over the central andes. *Monthly Weather Review*, *127*(5), 901–921. https://doi.org/10.1175/1520-0493(1999)127<0901:maotsp>2.0.co;2

Garreaud, R., Vuille, M., Compagnucci, R., & Marengo, J. (2009). Present-day South American climate. *Palaeogeography, Palaeoclimatology, Palaeoecology*, *281*(3), 180–195. https://doi.org/10.1016/j.palaeo.2007.10.032

Guan, B. (2020). *Arcatalog*. Retrieved from https://ucla.app.box.com/v/ARcatalog

Guan, B., & Waliser, D. E. (2015). Detection of atmospheric rivers: Evaluation and application of an algorithm for global studies. *Journal of Geophysical Research: Atmospheres*, *120*(24), 12514–12535. https://doi.org/10.1002/2015JD024257

Guan, B., Waliser, D. E., & Ralph, F. M. (2018). An intercomparison between reanalysis and dropsonde observations of the total water vapor transport in individual atmospheric rivers. *Journal of Hydrometeorology*, *19*(2), 321–337. https://doi.org/10.1175/JHM-D-17-0114.1

Haug, E. W., Kraal, E. R., Sewall, J. O., Van Dijk, M., & Diaz, G. C. (2010). Climatic and geomorphic interactions on alluvial fans in the Atacama Desert, Chile. *Geomorphology*, *121*(3), 184–196. https://doi.org/10.1016/j.geomorph.2010.04.005

Hersbach, H., Bell, B., Berrisford, P., Hirahara, S., Horányi, A., Muñoz Sabater, J., et al. (2020). The era5 global reanalysis. *Quarterly Journal of the Royal Meteorological Society*, *146*(730), 1999–2049. https://doi.org/10.1002/qj.3803

Hoffmeister, D. (2017). *Meteorological and soil measurements of the permanent master weather station 13 – cerros de calate, Chile. CRC1211 Database (CRC1211DB)*. https://doi.org/10.5880/CRC1211DB.4

Houston, J. (2006). Variability of precipitation in the Atacama Desert: Its causes and hydrological impact. *International Journal of Climatology*, *26*(15), 2181–2198. https://doi.org/10.1002/joc.1359

Houston, J., & Hartley, A. J. (2003). The central Andean west-slope rainshadow and its potential contribution to the origin of hyper-aridity in the atacama desert. *International Journal of Climatology*, *23*(12), 1453–1464. https://doi.org/10.1002/joc.938

Jacques-Coper, M., Falvey, M., & Muñoz, R. C. (2015). Inter-daily variability of a strong thermally-driven wind system over the Atacama Desert of South America: Synoptic forcing and short-term predictability using the GFS global model. *Theoretical and Applied Climatology*, *121*(1), 211–223. https://doi.org/10.1007/s00704-014-1231-y

Jones, D. L., Olivera-Ardid, S., Klumpp, E., Knief, C., Hill, P. W., Lehndorff, E., & Bol, R. (2018). Moisture activation and carbon use efficiency of soil microbial communities along an aridity gradient in the Atacama Desert. *Soil Biology and Biochemistry*, *117*, 68–71. https://doi.org/10.1016/j.soilbio.2017.10.026

Jordan, T. E., Herrera, H., Godfrey, L. V., Colucci, S. J., Gamboa, C., Urrutia, J., et al. (2019). Isotopic characteristics and paleoclimate implications of the extreme precipitation event of march 2015 in northern chile. *Andean Geology*, *46*(1), 1–31. https://doi.org/10.5027/andgeoV46n1-3087

Knippertz, P., & Martin, J. E. (2007). A pacific moisture conveyor belt and its relationship to a significant precipitation event in the semiarid southwestern united states. *Weather and Forecasting*, *22*(1), 125–144. https://doi.org/10.1175/WAF963.1

Montecinos, A., & Aceituno, P. (2003). Seasonality of the ENSO-related rainfall variability in Central Chile and associated circulation anomalies. *Journal of Climate*, *16*(2), 281–296. https://doi.org/10.1175/1520-0442(2003)016<0281:soterr>2.0.co;2

Pliscoff, P., Zanetta, N., Hepp, J., & Machuca, J. (2017). *Efectos Sobre La Flora Y Vegetación Del Evento De Precipitación Extremo De Agosto 2015 En Alto Patache, Desierto De Atacama, Chile* (Vol. *68*, pp. 91–103). (pp. 91–103). Revista de geografía Norte Grande. https://doi.org/10.4067/S0718-34022017000300091

Ralph, F. M., Dettinger, M. D., Cairns, M. M., Galarneau, T. J., & Eylander, J. (2018). Defining "Atmospheric River": How the Glossary of Meteorology Helped Resolve a Debate. *Bulletin of the American Meteorological Society*, *99*(4), 837–839. https://doi.org/10.1175/BAMS-D-17-0157.1

Ramsay, S., Amico, P., Bezawada, N., Cirasuolo, M., Derie, F., Egner, S., et al. (2020). The ESO Extremely Large Telescope instrumentation programme. In S. C. Ellis, & C. d'Orgeville (Eds.), *Advances in Optical Astronomical Instrumentation 2019* (Vol. *11203*, pp. 1–4). SPIE. https://doi.org/10.1117/12.2541400

Reyers, M. (2018). *WRF output daily accumulated total precipitation 10km resolution Atacama. CRC1211 Database (CRC1211DB)*. https://doi.org/10.5880/CRC1211DB.20

Reyers, M., Böhm, C., Knarr, L., Shao, Y., & Crewell, S. (2020). Synoptic-to-regional scale analysis of rainfall in the Atacama Desert (18°S–26°S) using a long-term simulation with WRF. *Monthly Weather Review*, 1–51. https://doi.org/10.1175/MWR-D-20-0038.1

Ritter, B., Wennrich, V., Medialdea, A., Brill, D., King, G., Schneiderwind, S., et al. (2019). Climatic fluctuations in the hyperarid core of the atacama desert during the past 215 ka. *Scientific Reports*, *9*(1), 5270. https://doi.org/10.1038/s41598-019-41743-8

Ruhm, J., Böhnert, T., Weigend, M., Merklinger, F. F., Stoll, A., Quandt, D., & Luebert, F. (2020). Plant life at the dry limit—Spatial patterns of floristic diversity and composition around the hyperarid core of the Atacama Desert. *PLoS One*, *15*(5), 1–21. https://doi.org/10.1371/journal.pone.0233729

Stein, A. F., Draxler, R. R., Rolph, G. D., Stunder, B. J. B., Cohen, M. D., & Ngan, F. (2016). NOAA's HYSPLIT Atmospheric Transport and Dispersion Modeling System. *Bulletin of the American Meteorological Society*, *96*(12), 2059–2077. https://doi.org/10.1175/BAMS-D-14-00110.1

Stohl, A., Forster, C., & Sodemann, H. (2008). Remote sources of water vapor forming precipitation on the Norwegian west coast at 60n–a tale of hurricanes and an atmospheric river. *Journal of Geophysical Research: Atmospheres*, *113*(D5), D05102. https://doi.org/10.1029/2007JD009006

Vargas, G., Rutllant, J., & Ortlieb, L. (2006). Enso tropical–extratropical climate teleconnections and mechanisms for holocene debris flows along the hyperarid coast of western South America (17°–24°s). *Earth and Planetary Science Letters*, *249*(3), 467–483. https://doi.org/10.1016/j.epsl.2006.07.022

Walk, J., Stauch, G., Reyers, M., Vásquez, P., Sepúlveda, F. A., Bartz, M., et al. (2020). Gradients in climate, geology, and topography affecting coastal alluvial fan morphodynamics in hyperarid regions–The atacama perspective. *Global and Planetary Change*, *185*, 102994. https://doi.org/10.1016/j.gloplacha.2019.102994